CHAPTER VI
ANTI-CORROSION PACKAGING FABRICATED BY POLYLACTIDE/VAPOR INHIBITOR MODIFIED MAGNETIC PCH NANOCOMPOSITE

6.1 Abstract

Polylactide/VCI modified magnetic PCH nanocomposites were prepared via direct melt intercalation by twin screw extruder. Polyethylene glycol was used as a plasticizer to improve the dispersion of VCI modified magnetic PCH in PLA matrix. Magnetic PCH-VCIs were utilized as the inorganic filler in PLA nanocomposites. Subsequently, they were fabricated to thin sheet by compression molding machine. The nanocomposites were characterized by using XRD, DSC and TG-DTA. The T_g and T_m of PLA/5% wt PEG were lower than those of neat PLA. The thermal properties of PLA nanocomposites marginally increased with higher magnetic PCH-VCI content. From the XRD result, the structure of PLA nanocomposites with 1 %wt Magnetic PCH- 40 %wt VCI possibly showed good exfoliations. For the properties of PLA nanocomposites, the anticorrosion properties increased with higher magnetic PCH-VCI content while the mechanical properties decreased with higher magnetic PCH-VCI content due to the aggregation of magnetic PCH-VCIs. Moreover, the oxygen and moisture permeability of PLA nanocomposites decreased with increasing magnetic PCH-VCI contents due to gas barrier properties of the magnetic PCH-VCI providing tortuous path in the films owing to mesoporous materials.

keyword : porous clay heterostructures, polylactide, nanocomposites, vapor corrosion inhibitor.

6.2 Introduction

Polymer-clay nanocomposites have been a growing interest to development. Nanocomposites constitute a new class of material that involves nano-scale dispersion in a matrix. Nanocomposites have at least one ultrafine phase dimension, typically in the range of 1–100 nm, and exhibit improved properties when compared to micro- and macro-composites. Strong interfacial interactions between the

dispersed clay layers and the polymer matrix lead to enhanced mechanical, thermal and barrier properties of the virgin polymer [1]. The most commonly used clay to prepare nanocomposite is from the smectite group, such as montmorilonite (MMT). In this clay mineral the silicate layers are joined through relatively weak dipolar and Van der Waals forces and the cations Na^+ and Ca^{2+} located in the interlayers. These cations can be replaced by organic cations such as alkylammonium ions through an ionexchange reaction to provide an organophilic silicate. Nanocomposite can be obtained by direct polymer melt intercalation, where polymer chains are spread into the space between the clay layers and this can be done by conventional polymer processing techniques such as extrusion [2].

Polylactides or poly (lactic acid) (PLA) is one of the most promising materials since it is thermoplastic, biodegradable, biocompatible and has high-strength, high-modulus and good processability [3]. PLA is a linear aliphatic thermoplastic which can either be synthesized by condensation of lactic acid or ring opening polymerization of lactide which is produced by fermentation of dextrose which it self is gained from annually renewable resources like corn [4].

Many research efforts focus on the polylactide-clay nanocomposites. The nanocomposites were prepared by melt compounding with polyethylene glycol (PEG) as a plasticizer. Plasticizers are one of the useful additional materials. Because plasticizers add to polymer matrix increase the flowability, molecules of polymer matrix can easily intercalate between clay platelets [5].

Recently, Nanocomposite technology paves the way for packaging innovation in the flexible film industries, offering enhance properties such as greater barrier protection, increased shelf life and lighter-weight material. From this point of view, one of the goals of this work is to study the effect of various magnetic PCH-VCI contents in PLA matrix. These as-synthesized mesoporous materials were blended with polylactide and the properties concerning the capability of polylactide/magnetic PCH-VCIs nanocomposites were tested. From the corrosion testing, magnetic PCH-VCIs can improve the anti-corrosion properties of PLA nanocomposite.

6.3 Experimental

Materials

Montmorillonite (MMT) was provided by Pai Kong Nano Technology Co., Ltd. The cation exchange capacity (CEC) of MMT is 102 mmol/100g of clay.

Cetyltrimethylammonium $[C_{16}H_{33}N^+(CH_3)_3]$ bromide (CTAB) was supplied by Fluka. Dodecylamine, $C_{12}H_{27}N$, (MW=185.35), (98% purified) was supplied by Aldrich. Tetraehtyl orthosilicate (TEOS), (MW=208.33), Ammonium hydroxide (NH_4OH), Ferric chloride hexahydrate $(FeCl_3.6H_2O)$ and Ferrous chloride tetrahydrate $(FeCl_2.4H_2O)$ were purchased from Fluka. Methanol (CH_3OH) was supplied by Lab Scan and Hydrochoric acid (HCl) was supplied by Carlo Erba. VCI 609 was provided by Optimal Technology Co., Ltd.

Polylactide 4042D (PLA) was supplied by NatureWorks Co., Ltd and Polyethylene glycol (PEG) was supplied by Sigma.

Purification and pH Adjustment of Na-Monmorillonite

Na-Monmorillonite was pulverized and sieve through 325 mesh. Three 10-g of the passing part were purified by centrifugation and then washed with distilled water until the pH value is near 7. After that, centrifugation was applied. Again, the same amount of distilled was added, and then the pH of each sample was adjusted to 9.0 by using dilute HCl and NaOH solutions. This procedure was repeated for 48 h to equilibrate the pH of each sample. The samples were air-dried overnight and again pulverized in a mortar.

Synthesis of Porous Clay Heterostructures (PCHs)

Na-Monmorillonite was converted into a Quqternary ammonium exchange form by ion exchange with cetyltrimethylammonium bromide and stirred at 50 °C for 24 h. After the reaction time, the solid was filtered out, washed with a mixture of methanol and water and then air-dried. The obtained organoclay was stirred in dodecylamine for 30 min at 50°C following which TEOS was added (at molar ratio of organoclay:dodecylamine:TEOS was 1:20:200). The resulting suspension was stirred for further 4 h at room temperature. The solid was separated from solution

again by filtration and air-dried overnight at room temperature to form the as-synthesized PCH. The surfactant was removed from the as-synthesized PCH by solvent extraction using methanol/HCL solution. Typically, 1 g of the as-synthesized PCH material has been added to 45 mL of methanol and 5 mL of HCl and refluxed for 2 h. The solid was subsequently filtrated out and washed with a mixture of methanol and water and air-dried at room temperature overnight.

Preparation of Magnetic PCHs

Ferric chloride hexahydrate and ferrous chloride tetrahydrate were used as iron sources which they were added in PCH at 20 wt%. Aqueous ammoniawas used as the precipitator. Distilled water was used as the solvent. Before the reaction, N_2 gas was flown through the reaction medium. The reaction was operated in a closed system to provide a nonoxidation environment. NH_4OH was slowly injected into PCH which added ferric chloride hexahydrate and ferrous chloride tetrahydrate under stirring 30 min. The dispersion was centrifuged at 3000 rpm for 20 min. After precipitation, the Fe_2O_3 particles in PCH were repeatedly washed and filtered before drying at room temperature in air atmosphere to form powders.

Preparation of Magnetic PCH-VCI

Vapor corrosion inhibitor was add in magnetic PCH at 40 wt% and stirred in ethanol which was used as the solvent at 50 °C for 30 min. The reaction was operated in a closed system to protect a volatility of VCI. After the reaction time, the solid was filtered out, washed with a mixture of methanol and water and then air-dried to form powders

Preparation of Nanocomposites

1, 2, 3, 4 and 5 wt% Magnetic PCH-40%wt VCI, 5 wt% PEG and PLA were melt blended in a co-rotating twin-screw extruder (Lab tech) with L/D=40/1 and D=20 mm; the processing conditions were the following: temperature (°C): 80, 150, 150, 160, 160, 165, 165,170,170, and 175°C from hopper to die, respectively and the screw rotation is 50 rpm. Each composition was premixed in a tumble mixer before introducing into the twin-screw extruder to be well mixed and extruded through a

single strand die, and solidified with cold water and pelletized. The obtained pellet was dried in oven.

Fabrication of Thin Sheet Nanocomposites

The nanocomposites films were prepared by compression molding machine. The nanocomposites pellets were dried in oven prior to compress. The compression molding was performed by using a Wabash V50H Press, at 195°C for 10 minutes and 25 tons compression force for 15 minutes before being cooled down to 50°C and thickness in the range of 0.1–0.3 mm.

Physical Measurements

TG-DTA curves were collected on a Perkin-Elmer Pyris Diamond TG/DTA instrument. The sample was loaded on the platinum pan and heated from 30°C to 500°C at a heating rate of 10°C/min under N_2 flows.

DSC analysis were carried out using a Perkin-Elmer DSC 7 instrument. The sample was first heated from 30°C to 180°C and cooled down at a rate of 10°C/min under a N_2 atmosphere with a flow rate of 60 ml/min. The sample was then reheated to 180°C at the same rate.

Scanning electron microscopy was performed on JEOL JSM-5410 lv Model. The specimens were coated with platinum under vacuum before observation to make them electrically conductive.

X-ray diffractometer was performed on Bruker AXS model D8 Discover with voltage 40 kV, current 40 mA, angle 0.7-10 degree/step and scan speed 0.5 sec/step.

Corrosion Test was investigated according to the Federal Standard No.101C, Method 4031 with a few modifications. The carbon steel test specimens were polished with the emery paper and were inserted in sealed film packages, and then submitted to the chamber. The chamber was a glass jar containing 45 ml of water/glycerin solution, with an airtight lid holding the carbon steel specimens.

Tensile Strength, elongation at break, stiffness and Young's modulus were measured according to ASTM D 882-91 using a LLOYD Mechanical Universal

Testing Machine with a 500 N load cell, a 10.00 mm/min crosshead speed and a
gauge length 50 mm. Test sample was cut into rectangular shape with a size of 10 x
150 mm and thickness in the range of 0.1-0.25 mm.

6.4 Results and Discussion

A. Thermal Properties of Nanocomposites

Melting temperatures of PLA and the nanocomposites are observed by DSC
heating scan thermograms in Table 6.1 and Figure 6.1. The neat PLA showed glass
transition temperature (T_g) at 64.0°C and the melting temperature (T_m) at 142.4°C.
After blending PLA with PEG as the plasticizer, the T_g and T_m of PLA/ 5%wt PEG
were lower than those of neat PLA. The T_g and T_m of PLA nanocomposites with
various Magnetic PCH-40%wt VCI content tend to increased as the higher content of
magnetic PCH-40%wt VCI.

(a)

(b)
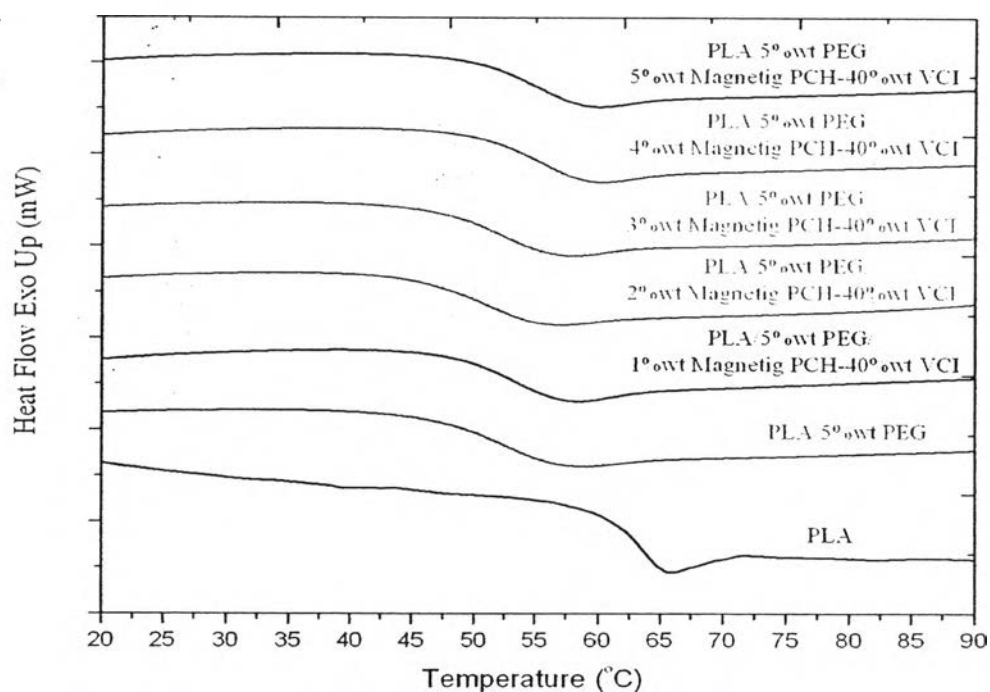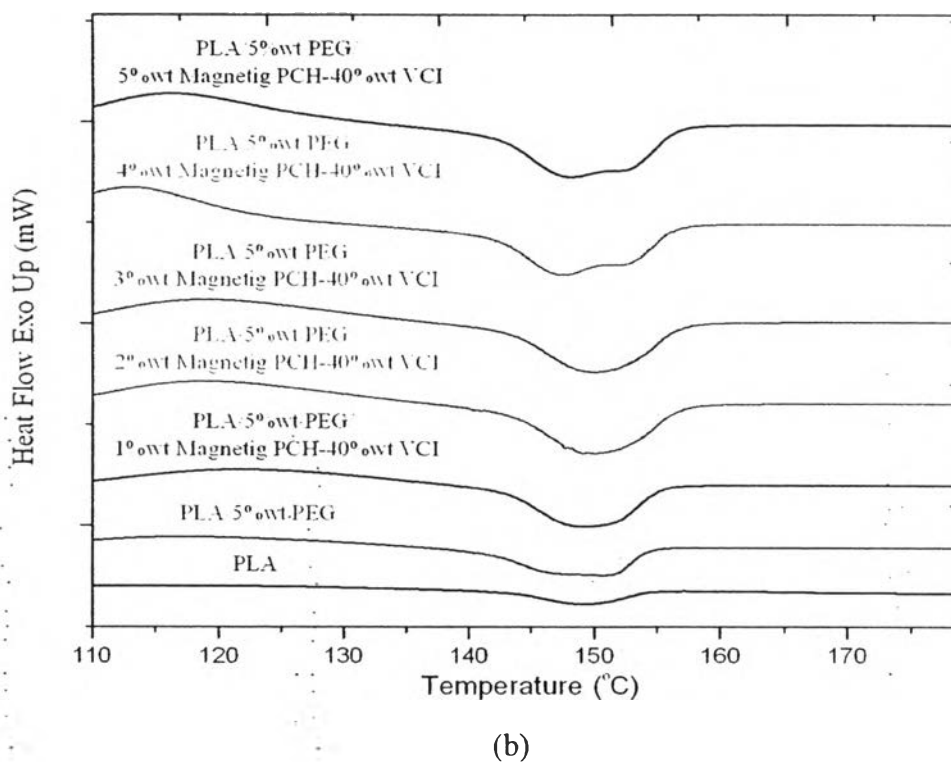
Figure 6.1 DSC heating scan thermograms of neat PLA, PLA/5%wt PEG and various PLA nanocomposites (a) Glass transition temperature and (b) Melting temperature.

TG-DTA curves of PLA and the nanocomposites are shown in Figure 6.2. The thermal degradation of PLA and all nanocomposites occured in single stage, and it indicated that thermal stability of the PLA nanocomposites were decreased when compared to neat PLA. The PLA nanocomposites marginally increased with the higher content of magnetic PCH-40%wt VCI. Generally, the shift considerably towards higher temperature may be attributed to the formation of a high-performance carbonaceous-silicate char, builds up on the surface [6]. The residue values of char were rather consistent with the amount of clay that had been added to the PLA. All results of thermal properties are listed in Table 6.1 and Figure 6.1-6.2.
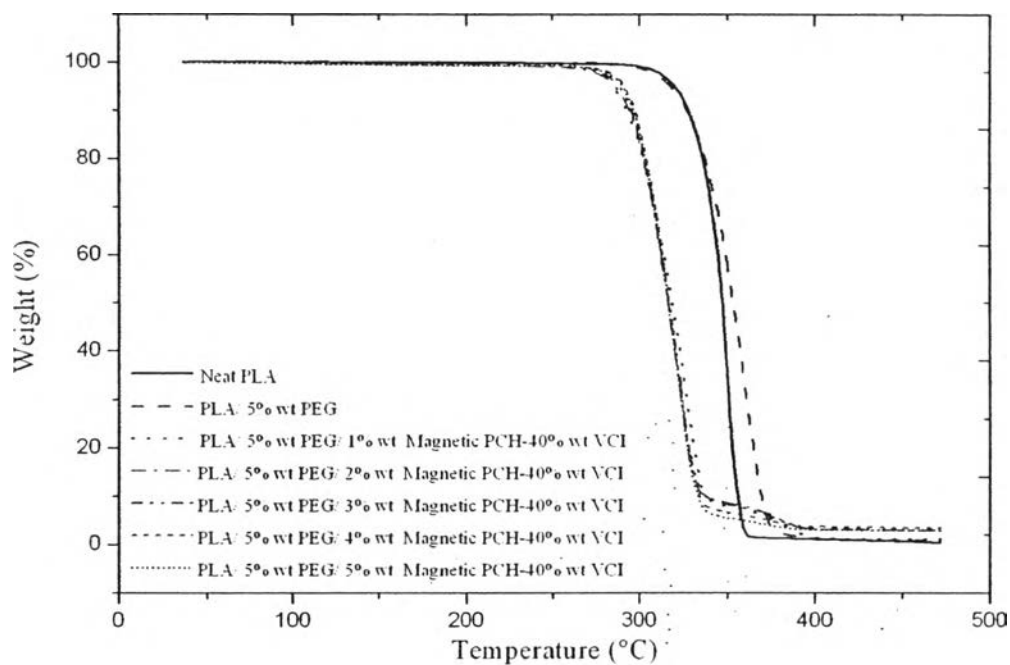
Figure 6.2 TG-DTA curves of neat PLA and various PLA nanocomposites.

Table 6.1 Thermal properties of neat PLA and PLA nanocomposites

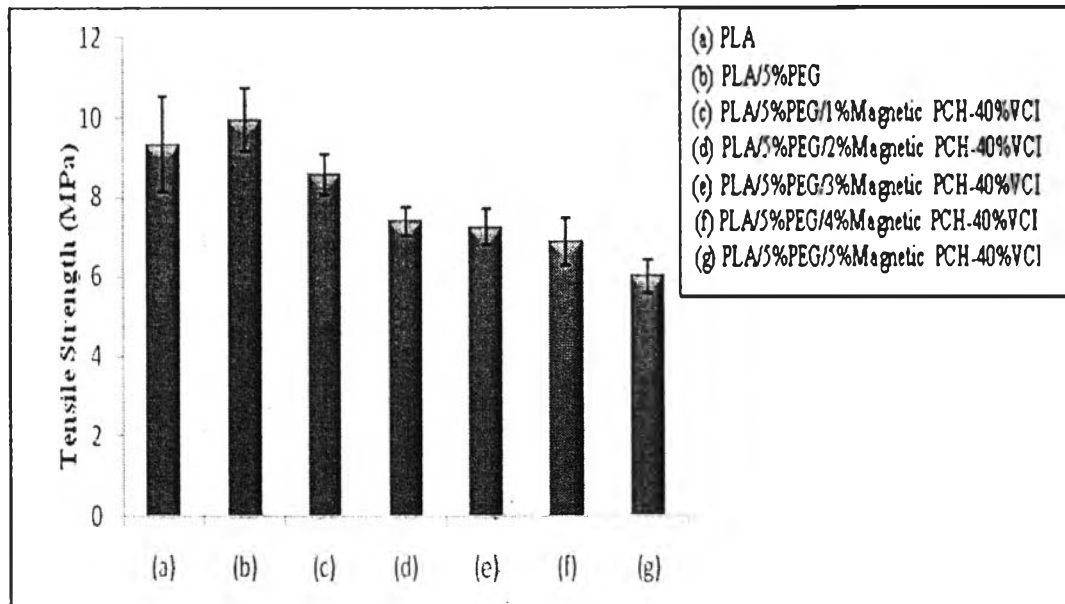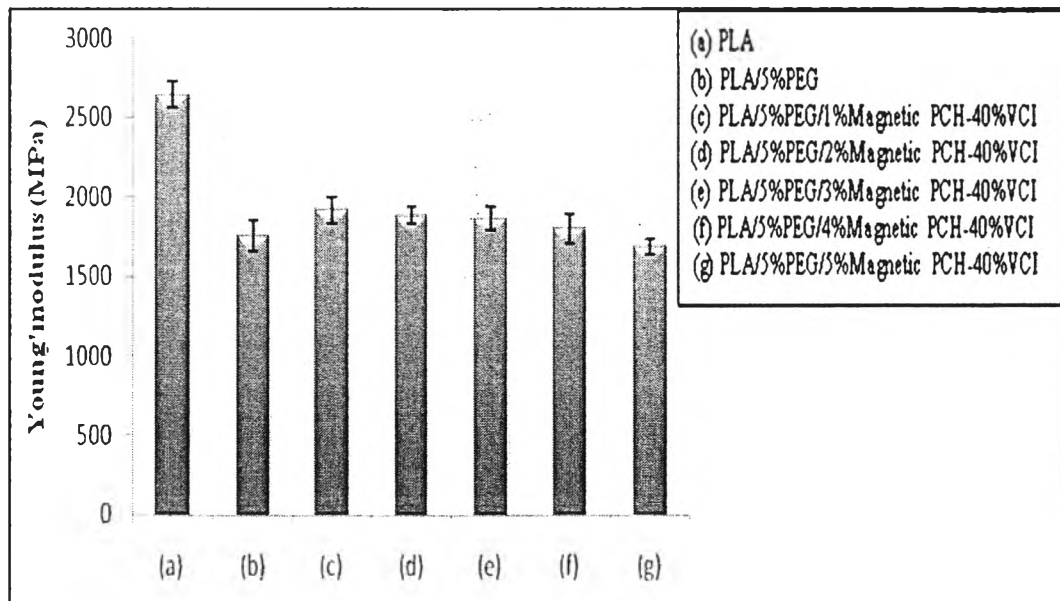| Sample	T_g (°C)	T_m (°C)	T_d (°C)	Char residue at 500 (°C)
PLA	64.0	142.4	345.3	1.3
PLA/ 5%wt PEG	46.6	139.9	334.0	1.6
PLA/ 5%wt PEG/ 1%wt magnetic PCH- 40%wt VCI	48.9	141.7	299.2	6.8
PLA/ 5%wt PEG/ 2%wt magnetic PCH- 40%wt VCI	48.2	141.9	299.8	7.2
PLA/ 5%wt PEG/ 3%wt magnetic PCH- 40%wt VCI	49.8	141.9	300.3	9.8
PLA/ 5%wt PEG/ 4%wt magnetic PCH- 40%wt VCI	49.7	142.1	300.7	10.3
PLA/ 5%wt PEG/ 5%wt magnetic PCH- 40%wt VCI	49.9	142.6	301.3	9.3

B. Mechanical measurement of PLA nanocomposites

The mechanical properties of neat PLA and PLA nanocomposites are shown in Table 6.2 and Figure 6.3. Tensile strength, young's modulus and % elongation at break of PLA nanocomposites decreased with the higher content of Magnetic PCH-40%wt VCI. The aggregation of magnetic PCH-VCIs affect to the mechanical properties of nanocomposites and the obstruction of magnetic PCH-40%wt VCI to the movement of PLA matrix was a reason in decline of mechanical properties with increasing magnetic PCH-40%wt VCI content which probably leads to lower polymeric chain mobility.

Table 6.2 Mechanical Properties of neat PLA and PLA nanocomposites
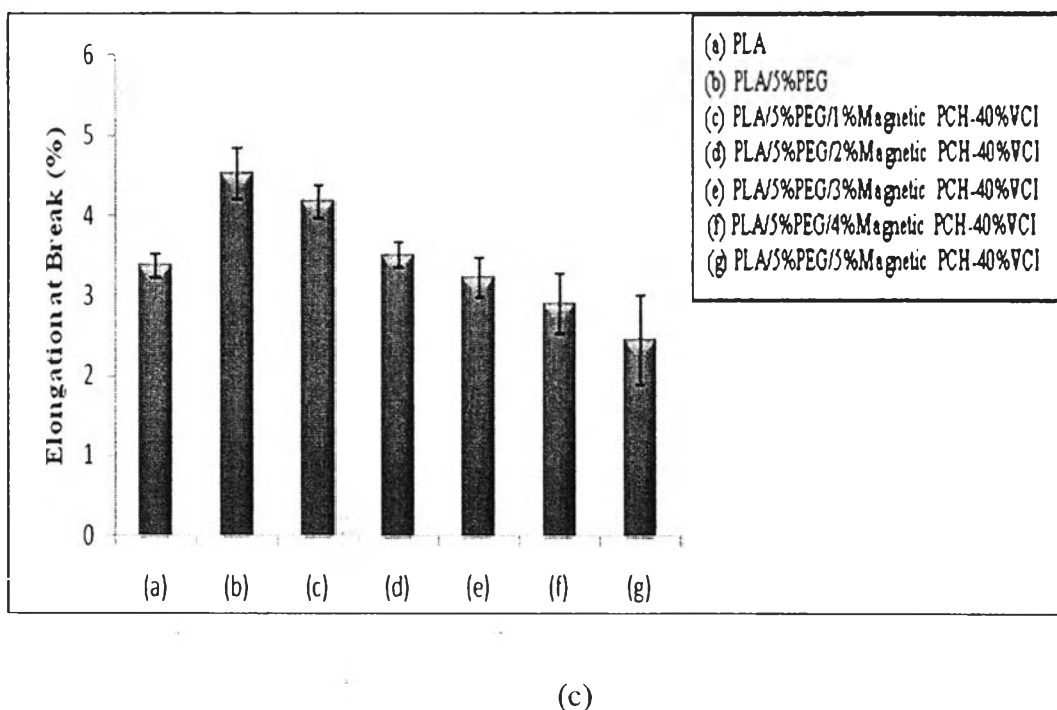
Sample	Tensile strength (MPa)	Elongation at Break (%)	Young's Modulus (MPa)
PLA	9.32 ± 1.20	3.38 ± 0.15	2641.89 ± 85.70
PLA/5%wt PEG	9.93 ± 0.80	4.53 ± 0.33	1751.49 ± 99.42
PLA/5%wt PEG/ 1% wt Magnetic PCH-40% wt VCI	8.58 ± 0.51	4.18 ± 0.20	1915.89 ± 83.68
PLA/5%wt PEG/ 2% wt Magnetic PCH-40% wt VCI	7.37 ± 0.36	3.50 ± 0.16	1884.07 ± 53.37
PLA/5%wt PEG/ 3% wt Magnetic PCH-40% wt VCI	7.24 ± 0.46	3.22 ± 0.25	1864.71 ± 71.38
PLA/5%wt PEG/ 4% wt Magnetic PCH-40% wt VCI	6.86 ± 0.59	2.90 ± 0.36	1798.76 ± 91.91
PLA/5%wt PEG/ 5% wt Magnetic PCH-40% wt VCI	5.99 ± 0.41	2.44 ± 0.55	1683.00 ± 47.63

Legend:
(a) PLA
(b) PLA/5%PEG
(c) PLA/5%PEG/1%Magnetic PCH-40%VCI
(d) PLA/5%PEG/2%Magnetic PCH-40%VCI
(e) PLA/5%PEG/3%Magnetic PCH-40%VCI
(f) PLA/5%PEG/4%Magnetic PCH-40%VCI
(g) PLA/5%PEG/5%Magnetic PCH-40%VCI

(a)

Legend:
(a) PLA
(b) PLA/5%PEG
(c) PLA/5%PEG/1%Magnetic PCH-40%VCI
(d) PLA/5%PEG/2%Magnetic PCH-40%VCI
(e) PLA/5%PEG/3%Magnetic PCH-40%VCI
(f) PLA/5%PEG/4%Magnetic PCH-40%VCI
(g) PLA/5%PEG/5%Magnetic PCH-40%VCI

(b)

(a) PLA
(b) PLA/5%PEG
(c) PLA/5%PEG/1%Magnetic PCH-40%VCI
(d) PLA/5%PEG/2%Magnetic PCH-40%VCI
(e) PLA/5%PEG/3%Magnetic PCH-40%VCI
(f) PLA/5%PEG/4%Magnetic PCH-40%VCI
(g) PLA/5%PEG/5%Magnetic PCH-40%VCI

(c)

Figure 6.3 Mechanical Properties of neat PLA and PLA nanocomposites with various Magnetic PCH-40%wt VCI content (a) Tensile Strength, (b) % Elongation at Break and (c) Young's Modulus.
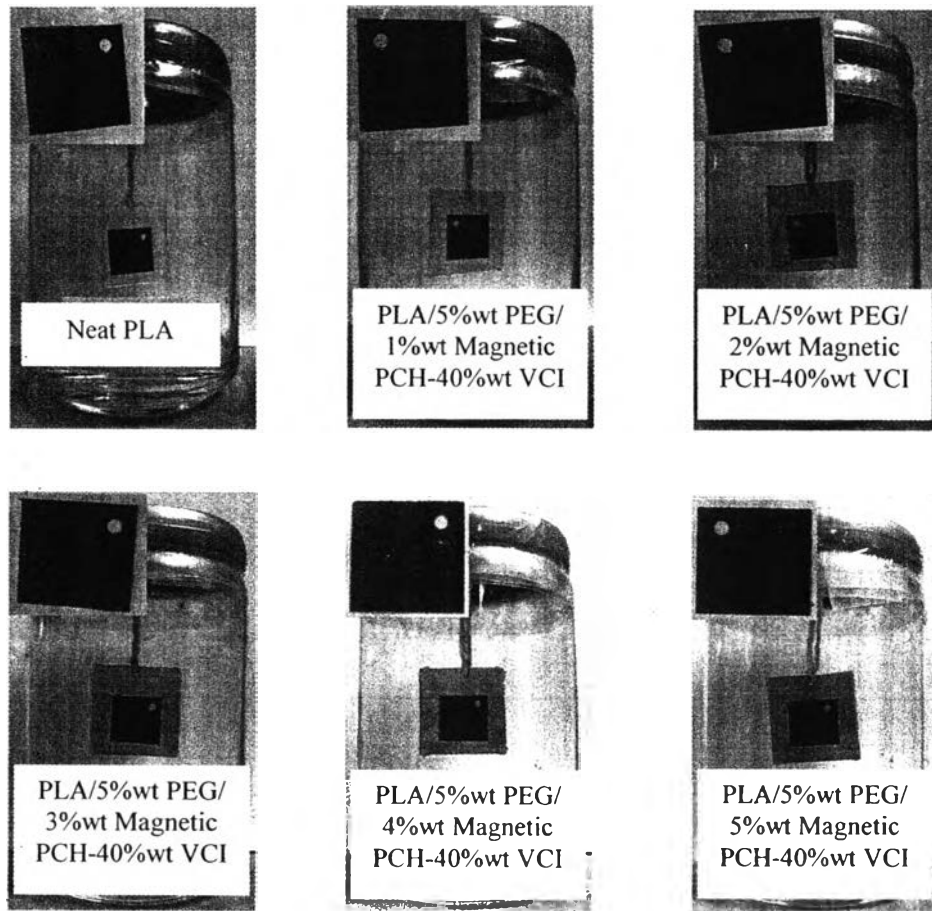
C. The Corrosion Test of PLA Nanocomposites

The corrosion test (86.5% RH at 20°C) of neat PLA and PLA nanocomposites were provided in Table 6.3, Figure 6.4, Figure 6.5 (before test) and Figure 6.6 (after test). The carbon steel specimen in neat PLA test had been corroded after 5 day and the carbon steel specimen in PLA nanocomposites test had lower corrosion rate with the higher content of Magnetic PCH-40 %wt VCI because VCI attaches itself to surface of carbon steel through weak chemical bonding and forms an adsorbed monolayer to shield this interface from penetration by corrosive agents such as water. Moreover, the higher magnetic PCH content can improve the moisture adsorptions in system.

Table 6.3 The first date of corrosion of carbon steel in neat PLA and PLA nanocomposites

Sample	The first date[(th)] of corrosion
PLA	5
PLA/ 5%wt PEG/ 1%wt magnetic PCH-40%wt VCI	18
PLA/ 5%wt PEG/ 2%wt magnetic PCH-40%wt VCI	19
PLA/ 5%wt PEG/ 3%wt magnetic PCH-40%wt VCI	19
PLA/ 5%wt PEG/ 4%wt magnetic PCH-40%wt VCI	21
PLA/ 5%wt PEG/5%wt magnetic PCH-40%wt VCI	23

(a)   (b)   (c)

(d)   (e)   (f)
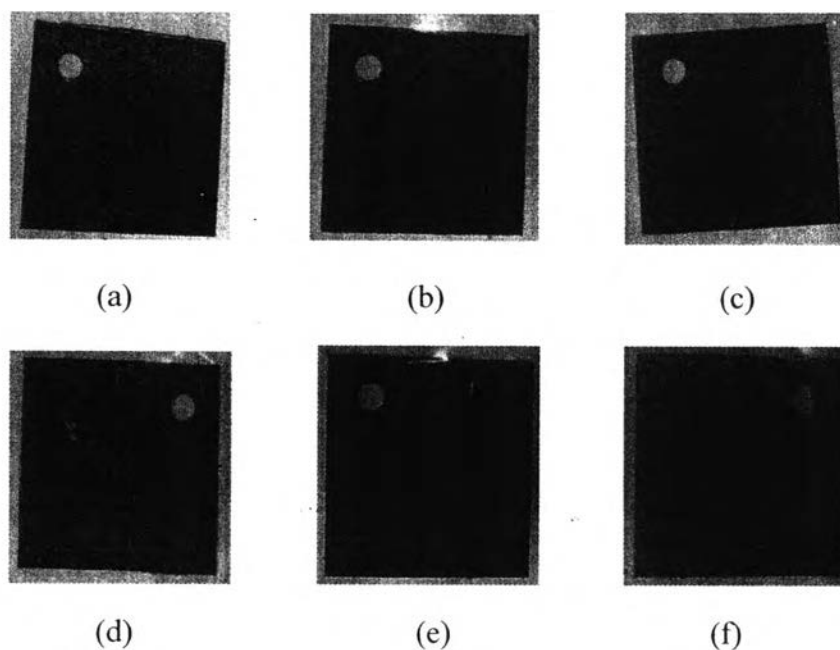
Figure 6.4 The carbon steel after corrosion test (86.5% RH at 20°C) of PLA nanocomposites (a) neat PLA, (b) 1%wt Magnetic PCH-40%wt VCI, (c) 2%wt Magnetic PCH-40%wt VCI, (d) 3%wt Magnetic PCH-40%wt VCI, (e) 4%wt Magnetic PCH-40%wt VCI and (f) 5%wt Magnetic PCH-40%wt VCI.

Figure 6.5 The corrosion before test (86.5% RH at 20°C) of neat PLA and PLA nanocomposites.
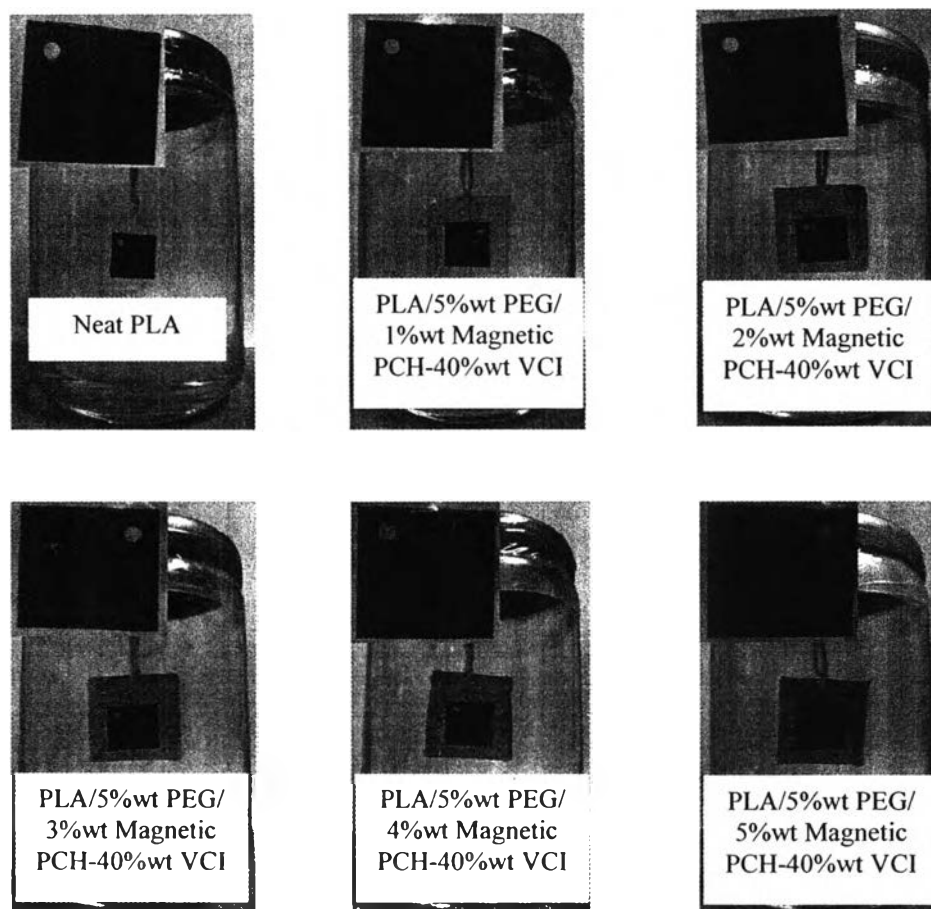
Figure 6.6 The corrosion after test (86.5% RH at 20°C) of neat PLA and PLA nanocomposites.

D. Dispersion of magnetic PCH in PLA nanocomposites

The phase separation of the nanocomposites between magnetic PCH-40%wt VCI and the PLA matrix was studied by scanning electron microscope (SEM). Figure 6.7(c) shows the surface of PLA/5%wt PEG/magnetic PCH-40%wt VCI which more roughness than the surface of PLA/5%wt. The magnetic PCH-40%wt VCI particles which were discernible as white spots on the surface of PLA matrix showed in Figure 6.7 (c).
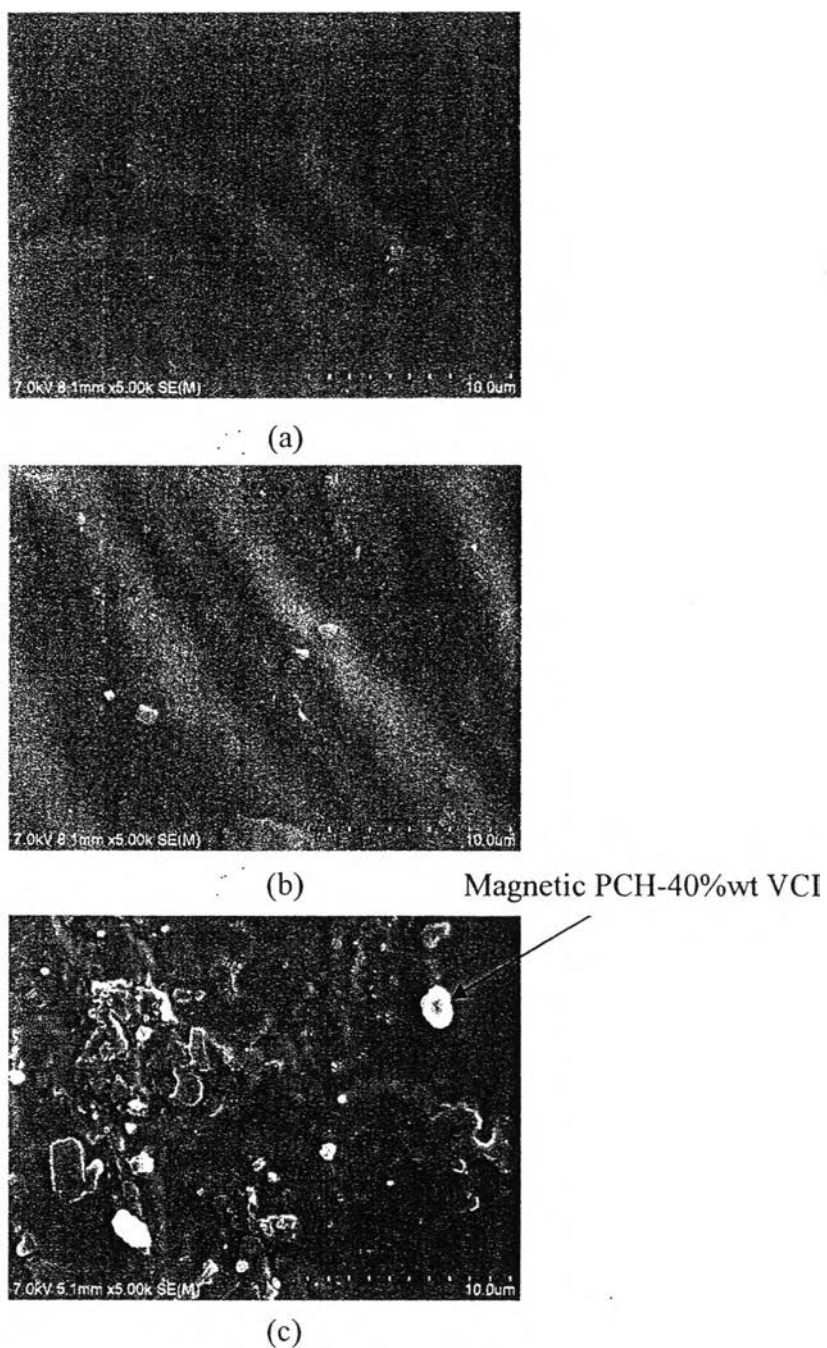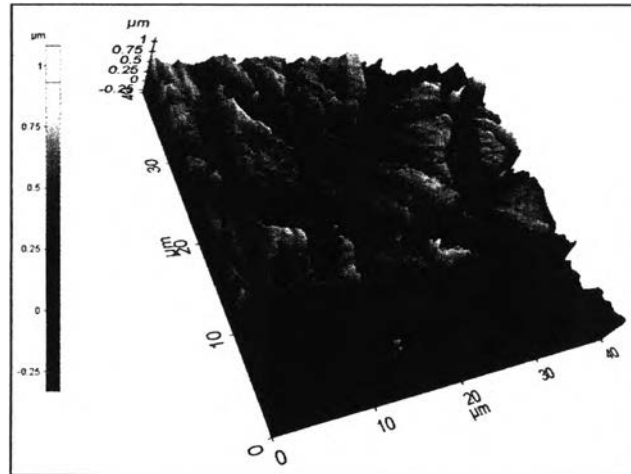
Figure 6.7 SEM images of PLA nanocomposites (a) neat PLA, (b) PLA/5% wt PEG and (c) PLA/5% wt PEG/1% wt Magnetic PCH-40%wt VCI.
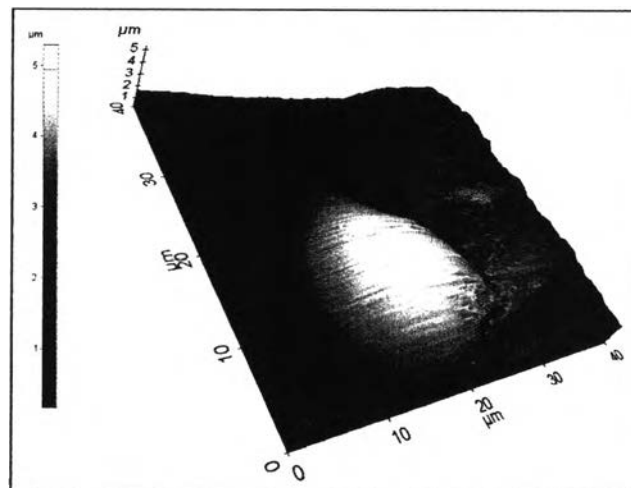
E. Surface of carbon steel in corrosion test

The surface of carbon steel from corrosion test (86.5% RH at 20°C) was provided in Figure 6.8. It reveals that surface of carbon steel was changed after

corrosion test from roughness to smooth surface because VCI attaches itself to surface of carbon steel and forms an adsorbed monolayer.
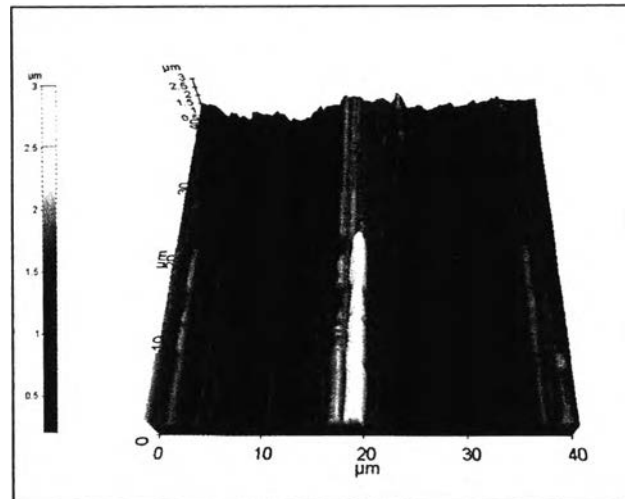

(a)

(b)

(c)

Figure 6.8 3D AFM images of carbon steel in corrosion test (86.5% RH at 20°C) (a) before testing, (b) after testing in Magnetic PCH-20%wt VCI powder and (c) after testing in Magnetic PCH-20%wt VCI film.

F. The structure of PLA nanocomposites

The structure of PLA nanocomposites is established using XRD diffraction analysis at low angle ($2\theta < 10°$). There is no peak observed in XRD results if clay platelets in polymer matrix are exfoliated [7]. The structures of Magnetic PCH-40 %wt VCI and PLA nanocomposites were provided in Figure 6.9 and Table 6.4. Neat PLA is no peak observed in XRD result [5]. However, Magnetic PCH-40 %wt VCI showed a strong peak at $2\theta = 1.70°$ (d = 51.90) as a standard data. The PLA nanocomposites which were added 1 %wt Magnetic PCH-40 %wt VCI are no peak observed. This suggested that good exfoliation possibly occurred in this material. On the contrary, The PLA nanocomposites which were added 3 and 5 %wt Magnetic PCH-40 %wt VCI are observed the strong peak at $2\theta = 1.36°$ (d = 64.88) and $2\theta = 0.94°$ (d = 93.87), respectively. This implied that the distance between clay platelets in PLA nanocomposite is larger than that Magnetic PCH-40 %wt VCI. Then, good exfoliation cannot be realized in these materials case because these peaks can be seen clearly [5].
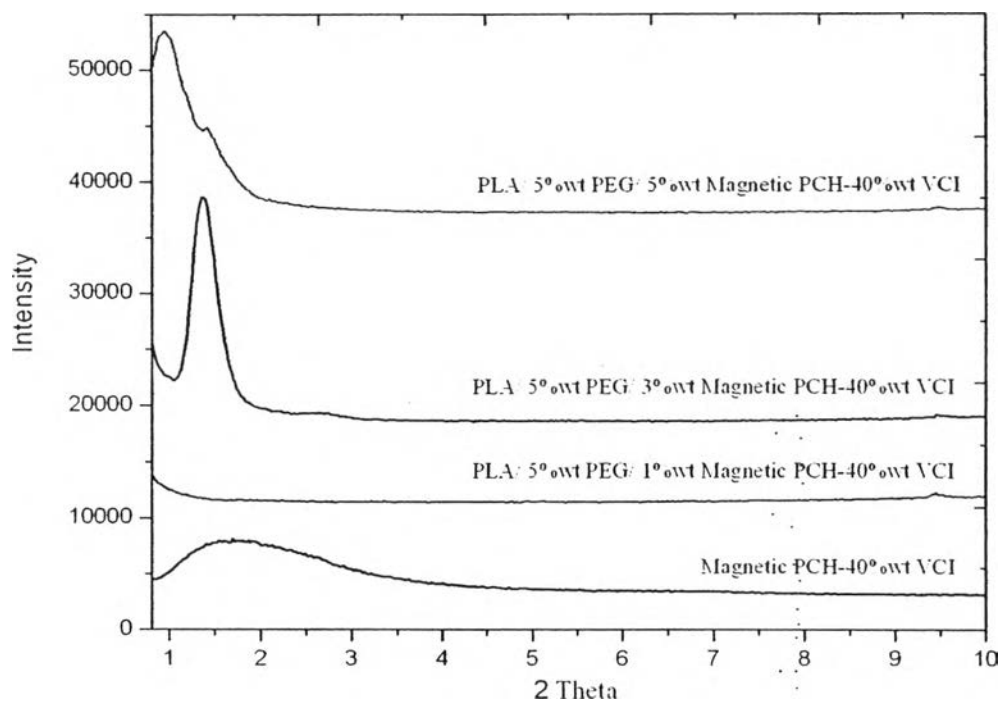
Figure 6.9 The XRD patterns of Magnetic PCH-40 %wt VCI and various PLA nanocomposites.

Table 6.4 The basal spacing of Magnetic PCH-40 %wt VCI and various PLA nanocomposites.

Sample	2θ (degree)	d-value (nm)
Magnetic PCH-40 %wt VCI	1.70	5.19
PLA/5%wt PEG/1%wt magnetic PCH-40%wt VCI	-	-
PLA/5%wt PEG/3%wt magnetic PCH-40%wt VCI	1.36	6.49
PLA/5%wt PEG/5%wt magnetic PCH-40%wt VCI	0.94	9.39

G. Oxygen Gas and moisture permeability of PLA nanocomposites

The migration of gases through materials has been a critical factor in the ability of packaging to increase the shelf life of products. Generally, the presence of nanoclay (high aspect ratio) in nanocomposites provides the improvement of gas barrier properties due to the hindered diffusion pathways through the nanocomposites [8]. Oxygen gas and moisture permeability of neat PLA, PLA/5%wt PEG and PLA nanocomposites sheets were summarized in Table 6.5 and 6.6. Magnetic PCH-40 %wt VCI improved gas barrier property of the sheet, indicating by lower oxygen gas and moisture permeability of the nanocomposites sheet. Improvement in barrier property was due to the presence of magnetic PCH-40 %wt VCI providing tortuous path in the films owing to these materials were combined with micro- and mesoporosity so gas molecules might be induced through these porous structures.

Table 6.5 Oxygen gas permeability of neat PLA, PLA/5%wt PEG and PLA nanocomposites

Sample	Oxygen gas permeability rate ($cc/m^2.d$)
PLA	103.5
PLA/5% wt PEG	92.7
PLA/ 5%wt PEG/ 1%wt PCH	90.0
PLA/ 5%wt PEG/ 1%wt magnetic PCH	89.4
PLA/ 5%wt PEG/ 1%wt magnetic PCH-40%wt VCI	87.4
PLA/ 5%wt PEG/ 2%wt magnetic PCH-40%wt VCI	84.2
PLA/ 5%wt PEG/ 3%wt magnetic PCH-40%wt VCI	84.2
PLA/ 5%wt PEG/ 4%wt magnetic PCH-40%wt VCI	80.9
PLA/ 5%wt PEG/ 5%wt magnetic PCH-40%wt VCI	73.8

Table 6.6   Moisture permeability of neat PLA, PLA/5%wt PEG and PLA nanocomposites

Sample	Moisture permeability rate ($g/m^2.d$)
PLA	62.4
PLA/5% wt PEG	51.3
PLA/ 5%wt PEG/ 1%wt PCH	48.0
PLA/ 5%wt PEG/ 1%wt magnetic PCH	45.5
PLA/ 5%wt PEG/ 1%wt magnetic PCH-40%wt VCI	42.0
PLA/ 5%wt PEG/ 2%wt magnetic PCH-40%wt VCI	40.8
PLA/ 5%wt PEG/ 3%wt magnetic PCH-40%wt VCI	37.7
PLA/ 5%wt PEG/ 4%wt magnetic PCH-40%wt VCI	36.8
PLA/ 5%wt PEG/ 5%wt magnetic PCH-40%wt VCI	33.0

6.5 Conclusions

Polylactide/VCI modified magnetic PCH nanocomposites were prepared via direct melt intercalation by twin screw extruder. Polyethylene glycol was used as a plasticizer to improve the dispersion of VCI modified magnetic PCH in PLA matrix. Subsequently, they were fabricated to thin sheet by compression molding machine. For the properties of PLA nanocomposites, the thermal properties of PLA nanocomposites marginally increased with higher magnetic PCH-VCI content. From the XRD result, the structure of PLA nanocomposites with 1 %wt Magnetic PCH- 40 %wt VCI possibly showed good exfoliations. On the contrary, PLA nanocomposites with 3 and 5 %wt Magnetic PCH- 40 %wt VCI showed the intercalations. After testing the corrosion, surface of carbon steel specimens was changed from roughness to smooth surface. This showed the layer of VCI on the carbon steel surface. The anticorrosion properties increased with higher magnetic PCH-VCI content while the

mechanical properties decreased with higher magnetic PCH-VCI content due to the aggregation of magnetic PCH-VCIs. Moreover, the oxygen and moisture permeability of PLA nanocomposites decreased with increasing magnetic PCH-VCI content due to gas barrier properties of the magnetic PCH-VCI providing tortuous path in the films.

6.6 Acknowledgements

6.7 References

[1]   Ishii, R., Nakatsuji, M., and Ooi, K. Micropor. Mesopor. Mater. 79 (2005) 111.

[2]   Galarneau, A., Barodawalla, A., and Pinnavaia, T.J. Nature 374 (1995) 529.

[3]   Drumright, R.E., Gruber, P.R., and Henton, D.E Advanced Materials 12 (2000) 1841.

[4]   Bax, B., Mussig, J. Composites Science and Technology 68 (2008) 1607.

[5]   Shui Tanoue, Aniwat Hasook, Yoshiyuki Iemoto Department of Materials Science and Engineering, University of Fukui, 3-9-1 Bunkyo, Fukui 910-8507, Japan

[6]   L.R.M. Estevao, R.S.V. Nascimento. Corrosion Science., 43., 1133-1153

[7]   Da-quan Zhang, Zhong-xun An, Qing-yi Pan, Li-xin Gao, Guo-ding Zhou. Applied Surface Science 253 (2006) 1343–1348.

[8]   LeBaron, P.C., Wang, Z., and Pinnavaia, T.J., Applied Clay Science 15 (1999) 11.

[9]   Modesti, M., Lorenzetti, A., Bon, D., and Besco, S. Polymer Degradation and Stability 91 (2006) 672.

[10]   M. Alexandre and P. Dubois, Material Science, 28, (2000) 1.

[11]   Lertwimolnun, W., and Vergnes, B. Polymer 46 (2005) 3462.

[12]   Shah, R.K., Hunter, D.L. and Paul, D.R. Polymer. 46 (2005) 2646.

[13]   Sinha Ray, S., and Okamoto, M. Prog. Polym. Sci. 28 (2003) 1539.

[14]   LeBaron, P.C., Wang, Z., and Pinnavaia, T.J., Applied Clay Science 15 (1999) 11.

[15]   Seephueng, A., Magaraphan, R., Nithitanakul, M., and Manuspiya, H. Proceeding of the 14 [th] PPC Symposium on Petroleum, Petrochems, and Polymers. (2008).

[16]   Polverejan, M., Liu, Y., and Pinnavaia, T.J. Chem. Mater. 14 (2002) 2283.

[17]   Zhu, H.Y., Ding, Z., and Barry, J.C. J. Phys.Chem. B. 106 (2002) 11420.

[18]   Ramos Filho, F.G., Melo, T.A., Rabello, M.S., and Silva, S.M., Polymer Degradation and Stability 89 (2005) 383.

[19]   Perrin-Sarazin, F., and Ton-That, M.T., Bureau, M.N., and Denault, J., Polymer 46 (2005) 11624.

[20]   Alexandre, M. and Dubois, P. Materials Science and Engineering 28 (2000) 63.